ARTICLES

Multiconfiguration Time-Dependent Hartree Dynamics on an ab Initio Reaction Surface: Ultrafast Laser-Driven Proton Motion in Phthalic Acid Monomethylester

H. Naundorf,[†] G. A. Worth,[‡] H.-D. Meyer,[§] and O. Kühn*,[†]

Institut für Chemie, Physikalische und Theoretische Chemie, Freie Universität Berlin, Takustrasse 3, D-14195 Berlin, Germany, Department of Chemistry, King's College London, The Strand, London WC2R 2LS, U.K., and Theoretische Chemie, Physikalische-Chemisches Institut, Universität Heidelberg, Im Neuenheimer Feld 229, 69120 Heidelberg, Germany

Received: September 28, 2001

The intramolecular nuclear wave packet dynamics of carboxy-deuterated phthalic acid monomethylester following excitation of the OD stretching vibration in the hydrogen bond is investigated. When one starts from a Cartesian reaction surface Hamiltonian, a nine-dimensional model is identified, which comprises the most strongly coupled degrees of freedom. The anharmonic coupling is demonstrated to lead, in particular, to low-frequency modulations of the OD dynamics. Partial vibrational energy randomization takes place on a time scale of 2 ps, which was not seen in earlier single configuration calculations.

1. Introduction

The dynamics of protons in intra- or intermolecular hydrogen bonds or hydrogen-bonded networks not only is of high relevance in many biological and chemical processes but also continues to be a challenge for theoretical models of interaction potentials and many particle dynamics.[1,2,3] Recently, there has been considerable progress in quantum chemistry, and in particular, the density functional method supplemented with modern exchange-correlation functionals has paved the road to study equilibrium structures and reaction pathways for intramolecular proton transfer in fairly large molecules. More flexibility concerning the exploration of the potential energy surface (PES) away from minimum energy pathways is provided by "on the fly" molecular dynamics methods.[4] This approach is nevertheless only suitable, at modest effort, in the limit of classical nuclear dynamics. An extension that includes quantum effects via imaginary time path integrals has been given for the calculation of statistical properties.[4]

Nonequilibrium quantum dynamics in real time, however, requires a priori knowledge of the underlying PES. There is little hope that the exact PES for more than three to four atomic molecules will routinely become available. This necessitates approximate schemes, the most successful being the reaction surface approach.[5,6] Here, full dimensionality is retained, but only selected reaction coordinates are treated exactly. For the case of an A−H···B hydrogen bond, for instance, this could be the A−H bond length. The majority of degrees of freedom (DOF) such as the A···B distance, however, are considered within the harmonic approximation. In fact, the reaction surface idea can be viewed as an extension of the reaction path (i.e., minimum energy path) concept.[7,8,9] It is more suitable, however, for heavy−light−heavy reactions in which the minimum energy path can be sharply curved.

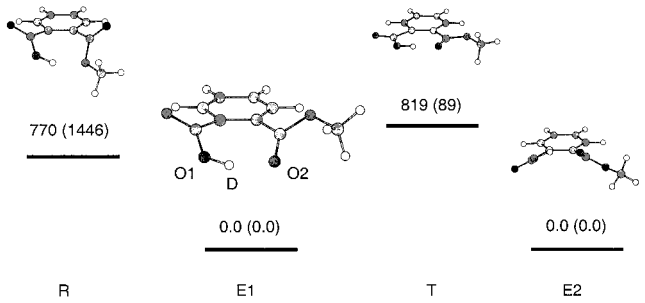

Figure 1. Various conformations of PMME. Numbers refer to relative energies in cm^{-1} obtained at the MP2 (DFT/B3LYP) level of theory with a Gaussian 6-31+(d,p) basis set.

There has been a long discussion about the nature of the normally broad and often structured linear absorption bands of A−H stretching vibrations in solution after formation of an A−H···B hydrogen bond. It is well accepted that the anharmonic coupling between the high-frequency A−H and the low-frequency A···B bridge vibration is important. Whether the solvent couples dominantly to the A−H or the A···B vibration as well as the strength of this interaction compared to the anharmonic coupling determines the band shape. Strong anharmonicities in particular can lead to vibrational combination transitions (Franck−Condon like progressions) with respect to the low-frequency mode, which might be hidden underneath a broad band.[10−13] Experimentally, this issue can be addressed by time-resolved nonlinear spectroscopy. Recently, Stenger et al.[14,15] used ultrafast IR pump−probe spectroscopy to demonstrate coherent vibrational dynamics upon excitation of the O−D band of carboxy-deuterated phthalic acid monomethyl ester (PMME-D) shown in Figure 1. The observed periodic modulations of the signals have been assigned to a low-frequency

* To whom correspondence should be addressed.
[†] Freie Universität Berlin.
[‡] King's College London.
[§] Universität Heidelberg.

10.1021/jp013652y CCC: $22.00
Published on Web 01/12/2002

normal mode, which by virtue of the anharmonicity of the PES influences the O−O distance across the hydrogen bond. In ref 16, we gave support for this experimental suggestion by combining a full-dimensional ab initio reaction surface Hamiltonian with a time-dependent self-consistent field (TDSCF)[17,18] dynamics simulation. In particular, it has been found that two vibrational modes are strongly coupled to the O−D dynamics; that is, besides a low-frequency (∼70 cm^{-1}) mode, we identified an important high-frequency (∼1000 cm^{-1}) mode of which the dynamical signatures, however, cannot be resolved at the present experimental time resolution. On the basis of the TDSCF dynamics, it had been concluded in ref 16 that the experimentally observed T_1 relaxation time of 400 fs cannot be due to intramolecular energy randomization.

In the present contribution, we will use the Cartesian reaction surface (CRS) Hamiltonian together with multiconfiguration time-dependent Hartree (MCTDH) wave packet propagation[21] to study the dynamics of PMME-D excited by an ultrafast laser pulse. The CRS Hamiltonian is ideal for combination with the MCTDH method, and together, they provide a powerful tool for the study of quantum dynamics of molecular systems. In section 2, we introduce the model system PMME-D and give details of the reaction surface Hamiltonian. In section 3, the MCTDH method is briefly reviewed putting emphasis on the implementation of explicitly time-dependent Hamiltonians. Numerical results extending our previous studies[16] are discussed in section 4, and the paper is summarized in section 5.

2. Reaction Surface Hamiltonian

Several stable configurations of PMME-D can be identified by geometry optimization (all quantum chemistry calculations have been performed using the Gaussian 98 program package[22]); only the lowest energetic ones are shown in Figure 1. The most stable geometry obtained with second-order Møller−Plesset perturbation theory (MP2) and a Gaussian 6-31+(d,p) basis set is denoted **E1** in Figure 1. There is an isoenergetic enantiomer (**E2**) separated by a barrier of 819 cm^{-1} at **T** from **E1**, to which it is related by reflection through the plane of the ring. Out of the higher energetic isomers, the most notable is the rotamer **R** with respect to the ester group. We have also performed geometry optimizations using density functional theory with the B3LYP exchange-correlation functional and the respective energy differences are also given in Figure 1. Density functional theory predicts **E1** to be more planar than the MP2 structure (for a more detailed comparison, see also ref 16), which is responsible for the remarkable differences in the energies of the **R** and **T** configurations.

Configuration **E1** will be the starting point for the construction of a reaction surface for the dynamics of the intramolecular hydrogen bond, O1−D···O2. The position of the deuterium within the molecular frame can, in principle, be described either in internal[5,6] or in Cartesian[23] coordinates. A CRS Hamiltonian has the numerical advantage that the couplings between the different DOF are part of the potential energy operator. This implies that, in contrast to internal-coordinate-based reaction surfaces, there is no numerical reason to invoke an adiabatic approximation.[6] The CRS Hamiltonian can be established by identifying relevant Cartesian reaction coordinates as well as a suitable reference geometry for the substrate atoms. In the present case, the choice is obvious, that is, the anharmonicity of the deuterium's motion along the O1−D bond (here, the x direction) needs to be accounted for while the remaining atoms are treated in harmonic approximation with respect to the geometry of **E1**. To follow refs 16 and 23, the CRS Hamiltonian will be expressed in terms of a zeroth-order part,

$$H_{\mathrm{CRS}}^{(0)} = H_{\mathrm{sys}} + H_{\mathrm{sub}} = \frac{{p_H}^2}{2m_H} + V(x) + \frac{1}{2}\sum_n [{p_n}^2 + {\omega_n}^2 {Q_n}^2] \tag{1}$$

which describes the one-dimensional reaction coordinate x and the uncoupled set of harmonic mass-weighted substrate modes $\{Q_n\}$, and an interaction part,

$$V_{\mathrm{CRS}} = -\sum_n f_n(x) Q_n + \frac{1}{2}\sum_{mn} (K_{mn}(x) - \delta_{mn}{\omega_n}^2) Q_n Q_m \tag{2}$$

Note that the zeroth-order substrate Hamiltonian has been defined with respect to the frequencies at the reference configuration, that is, ${\omega_n}^2 = K_{nn}(x_{\mathrm{eq}})$. Equation 2 contains two types of couplings, linear and quadratic, in the substrate coordinates. The former derives from the fact that on a CRS one does not necessarily move on a minimum energy path, that is, the n-th mode is shifted by a reorganization energy, $\Delta E_n(x) = {f_n}^2(x)/(2{\omega_n}^2(x))$ (neglecting the mode−mode coupling). As discussed in ref 24, the reorganization energy gives a convenient means for identification of those substrate modes that have the strongest impact on the reaction coordinate dynamics. The quadratic term in eq 2 leads to a mixing between different substrate normal modes, if the character of the normal modes changes along the reaction coordinate.

We will consider the dynamics of the O1−D stretching vibration as triggered by the interaction with an external laser field. When the dipole approximation is invoked, eqs 1 and 2 are supplemented by the time-dependent Hamiltonian

$$H_{\mathrm{field}}(t) = -d(x)E(t) \tag{3}$$

where $d(x)$ is the dipole moment operator along the reaction coordinate. For the classical electric field, we will use the form

$$E(t) = E_0 \Theta(\tau - t) \sin^2(\pi t/\tau) \cos(\Omega t) \tag{4}$$

with E_0, τ, and Ω being the amplitude, the duration, and the center frequency, respectively. The quantum chemistry input for the CRS Hamiltonian, eqs 1, 2, and 3, thus consists of the reference potential, the forces, the Hessian, and the dipole moment as a function of the reaction coordinate.

3. MCTDH with a Time-Dependent Hamiltonian

The theory and implementation of the MCTDH method for wave packet propagation have been detailed in a recent review,[21] and only an outline will be provided here. The basis of the method is to use a wave function expanded in a set of time-dependent single-particle functions (SPFs), $\{\varphi_j^{(\kappa)}\}$:

$$\begin{aligned}\Psi(x,Q_1,\ldots Q_p,t) &= \sum_{j_0=1}^{n_0} \cdots \sum_{j_p=1}^{n_p} A_{j_0 \cdots j_p}(t) \varphi_{j_0}^{(0)}(x,t) \prod_{\kappa=1}^{p} \varphi_{j_\kappa}^{(\kappa)}(Q_\kappa,t) \\ &= \sum_J A_J \phi_J \end{aligned} \tag{5}$$

The second line defines the multi-index J and the configurations ϕ_J. As written here, the SPFs are functions of a single DOF. In general, this does not need to be the case, and for large systems, such as the model studied here, it is more efficient to treat DOFs combined together using multidimensional SPFs. Note that each

"particle" may have different numbers of functions, which makes this ansatz very flexible.

Optimizing the time evolution of this wave function ansatz, using the Dirac−Frenkel variational principle,[25,26] leads to a set of coupled equations for the SPFs and wave function coefficients

$$i\dot{A}_J = \sum_L \langle \phi_J|H|\phi_L\rangle A_L \tag{6}$$

$$i\dot{\varphi}_a^{(\kappa)} = (1 - P^{(\kappa)})\sum_{b,c} \rho_{ab}^{(\kappa)^{-1}} \mathscr{H}_{bc}^{(\kappa)} \varphi_c^{(\kappa)} \tag{7}$$

where $P^{(\kappa)} = \sum_{j=1}^{n_\kappa} |\varphi_j^{(\kappa)}\rangle\langle\varphi_j^{(\kappa)}|$ is a projector that preserves the orthonormality of the single-mode functions, $\mathscr{H}^{(\kappa)}$ is a mean field operator matrix accounting for the other modes, and $\rho^{(\kappa)}$ is the reduced density matrix related to the populations of the SPFs. The last two terms can be best represented by introducing the single-hole functions, $\psi_j^{(\kappa)} = \langle\varphi_j^{(\kappa)}|\Psi\rangle$, which is simply all of the terms in the wave function with a particular SPF projected out. The mean-field operator matrix elements can now be written as $\mathscr{H}_{jk}^{(\kappa)} = \langle\psi_j^{(\kappa)}|H|\psi_k^{(\kappa)}\rangle$, and the density matrices become $\rho_{jk}^{(\kappa)} = \langle\psi_j^{(\kappa)}|\psi_k^{(\kappa)}\rangle$, which is in fact the sum of the squared coefficients for a combination of SPFs.

To implement the method, the SPFs are typically expanded in a time-independent basis set, such as a discrete variable representation (DVR),[27,28] although any suitable set may be used. If N DVR functions are used for the representation of the n SPFs of a particle, then when $N = n$, the standard numerically exact solution of the time-dependent Schrödinger equation is obtained. The variational basis of the MCTDH method, however, means that in general $n \ll N$, and this basis set contraction leads to a reduction of the computational effort, which can amount to several orders of magnitude for large systems. An important feature of the method is that at the lower limit of $n = 1$ the TDSCF method (also known as time-dependent Hartree)[17,18,25] is obtained. Thus, by varying n, the quality of a calculation can be varied from cheap and qualitative to accurate depending on needs and computer resources.

As written above, the method requires the evaluation of multidimensional integrals both for the time-derivative of the expansion coefficients and for building the mean-field operator matrices. Writing the operator as products of single-particle operators,

$$H(x,Q_1,...,Q_p;t) = \sum_{s=1}^{n_s} e_s(t) h_s^{(0)}(x) \prod_{\kappa=1}^{p} h_s^{(\kappa)}(Q_\kappa) \tag{8}$$

allows these integrals to be written as products of one-dimensional integrals, enabling very efficient routines to be used for this evaluation. The functions $e_s(t)$ define the time-dependence of the Hamiltonian, that is, $E(t)$ in eq 3. Note that an important feature of the CRS Hamiltonian, eqs 1 and 2, is that it comes in the desired product form, as does the time-dependent operator describing the interaction with the electric field, eq 3. The latter property has been used here to include the time-dependence of the driving laser field with minimal overhead—only the Hamiltonian expansion coefficients need to be recalculated at each step. The main problem introduced by the time-dependence of the Hamiltonian is that the efficient constant mean-field integration scheme[19] for propagating an MCTDH wave packet cannot be used. In this study, the equations of motion were integrated using a general purpose sixth order predictor−corrector scheme. Note, however, that the small step sizes required by the time-dependent operator are less of a disadvantage for the MCTDH method, which inherently requires small step sizes because of the nonlinear equations of motion, than it is to the standard methods, which rely on large step sizes for their efficiency. All wave packet calculations have been made using the Heidelberg MCTDH package.[20]

4. Numerical Results

In Figure 2A, the potential energy, $V(x)$, for the motion along the reaction coordinate and frozen substrate coordinates is shown together with the respective wave functions for the three lowest states, $\nu_{OD} = 0, 1, 2$, following from the solution of $H_{sys}|a\rangle = E_a|a\rangle$ on a grid as specified in Table 1. According to the shape of the rather anharmonic potential, the hydrogen bond can be classified to be of medium strength, that is, there will be *no* proton transfer. The importance of the different substrate normal modes for the hydrogen bond dynamics has been estimated by calculating their contribution to the reorganization energy at the representative position $x_{eq} + 0.2\dot{A}$ where its total value is 0.24 eV. In Figure 2B,C, we characterize two strongly coupled substrate modes, ν_1 and ν_{23}, by means of their vibrationally diabatic (VD) PES and displacement vectors. The VD PESs, $V_{aa}(Q_n)$, have been obtained from

$$\langle a|H_{sub} + V_{CRS}|a\rangle \approx \sum_n \left[\frac{{p_n}^2}{2} + \frac{1}{2}\langle a|K_{nn}(x)|a\rangle {Q_n}^2 - \langle a|f_n(x)|a\rangle Q_n\right] = \sum_n \left[\frac{{p_n}^2}{2} + V_{aa}(Q_n)\right] \tag{9}$$

that is, the mode coupling ($\propto K_{mn}(x)$) has been neglected. Equation 9 is the well-known shifted oscillator Hamiltonian.[30] The two modes in Figure 2B,C are of low ($\omega_1/(2\pi c) = 67$ cm^{-1}) and high ($\omega_{23}/(2\pi c) = 986$ cm^{-1}) frequency and represent motions that modify the hydrogen bond geometry. While these modes correspond to extreme cases (ν_{23}, strongest coupling; ν_1, lowest frequency), six more modes with reorganization energies greater than 6 meV (about 50 cm^{-1}) can be identified that also influence the hydrogen bond. These eight substrate modes comprise about 85% of the reorganization energy at $x_{eq} + 0.2\dot{A}$, see also Table 1. Together with the reaction coordinate, they constitute a nine-dimensional (9D) model, which will be used in the subsequent quantum dynamics calculations. The coupling between this 9D model and the remaining substrate modes is weak enough to be neglected on the time scale of 1−2 ps considered below.

In the wave packet simulations, we have made use of the mode combination method to increase the efficiency by reducing the size of the SPF basis set required because correlations within the combined modes are treated explicitly.[29] The reaction coordinate x has been combined with the strongest coupled mode ν_{23} using seven SPFs; the combinations for the other modes have been chosen on the basis of frequency matching, ν_1, (ν_3,ν_5), (ν_7,ν_9), (ν_{13},ν_{24}), and using five SPFs for each of these MCTDH particles. Thus, we have five MCTDH particles and a total of 4375 configurations for the MCTDH propagation. For numerical parameters, see also Table 1.

The number of SPFs per mode that need to be included depends on the propagation time as well as on the strength of the external field. For the field, we used the form given in eq 4 with $\Omega/(2\pi c) = 2430$ cm^{-1} (fundamental ν_{OD} transition in the 9D potential), $\tau = 300$ fs, and $E_0 = 5 \times 10^{-4}\ E_h/ea_B$. The dipole gradient at $x = x_{eq}$ was calculated to 1.55 D/a_B. For these parameters only, the fundamental transition of the reaction coordinate will be appreciably excited.

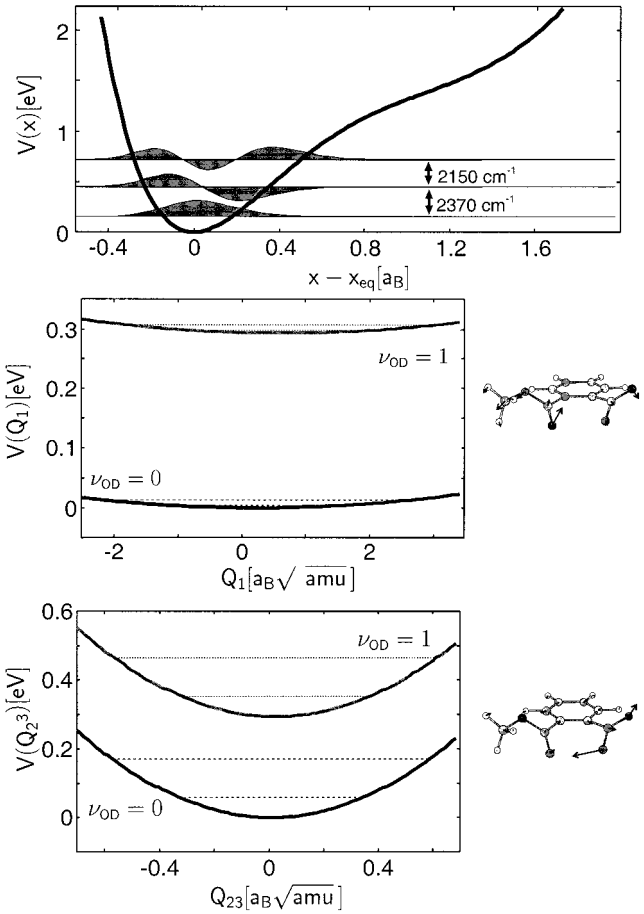

Figure 2. Potential energy $V(x)$ along the reaction coordinate (O1−D bond) and for a frozen substrate as obtained at the MP2 level of theory with a Gaussian 6-31+(d,p) basis set (A). Also shown are the wave functions for the three lowest eigenstates. In panels B and C, the VD potential for the motion of the ν_1 and ν_{23} mode, respectively, is shown together with the respective normal mode displacements (cf. eq 9).

TABLE 1: Parameters of the 9D Model Used in the MCTDH Simulations[a]

mode	$\omega_i/(2\pi c)$ (cm^{-1})	ΔE_n (eV)	SPF	grid	DVR
ν_{OD}	2370		7	−0.8/1.1	40
ν_{23}	985	1.273×10^{-1}		−100/100	40
ν_1	67	9.469×10^{-3}	5	−250/250	40
ν_3	147	8.572×10^{-3}	5	−205/225	32
ν_5	201	8.925×10^{-3}		−175/200	32
ν_7	263	1.758×10^{-2}	5	−175/175	32
ν_9	306	9.143×10^{-3}		−175/175	32
ν_{13}	507	1.216×10^{-2}	5	−150/150	32
ν_{24}	1011	7.537×10^{-3}		−125/125	32

[a] In the different rows, the DOF combined in each MCTDH particle are given. The grid dimensions are given in atomic units (mass-scaled for the substrate modes), and the last column shows the number of harmonic oscillator DVR functions used. (The grid for the reaction coordinate is given with respect to $x_{eq} = 1.85\ a_B$. ΔE_n is the reorganization energy at $x = x_{eq} + 0.2$Å.) Note that in the dynamics simulations the potential energy terms in eqs 1 and 2 as well as the dipole moment have been fitted to polynomials and powers of exponentials.

In Figure 3, the time-dependence of the expectation values for the reaction coordinate and the substrate modes ν_1 and ν_{23} is shown. For the reaction coordinate (panel B), we observe a rapid oscillation triggered by the driving field (panel A). The oscillation frequency corresponds to that of the $\nu_{OD} = 0 \rightarrow 1$ transition. It is interesting to note that initially we have $\langle x \rangle = 0.04\ a_B$, that is, a deviation from zero due to quantum description of the anharmonic PES. The dynamics of $\langle x \rangle$ covers the range

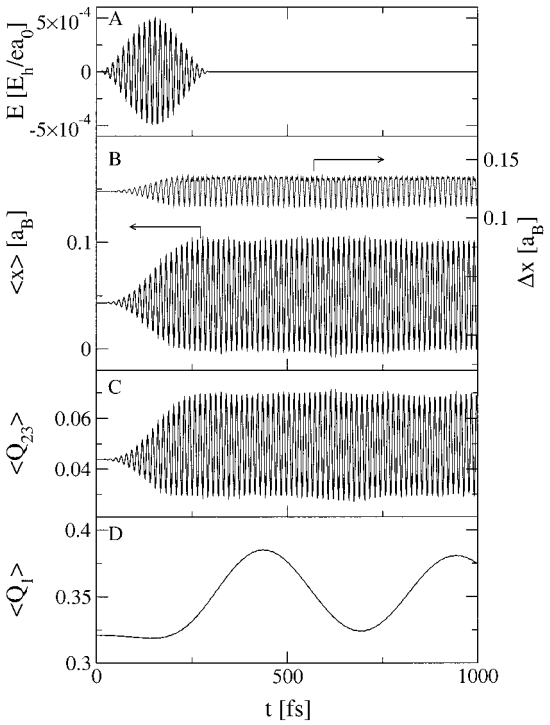

Figure 3. Time-dependence of the external driving field (A) in eq 4 ($\Omega/(2\pi c) = 2430$ cm^{-1}, $\tau = 300$ fs, and $E_0 = 5 \times 10^{-4}$ E_h/ea_B). In the lower panels, the time evolution of the coordinate expectation values for (B) the reaction coordinate (as well as its variance (upper curve)), (C) mode ν_{23}, and (D) mode ν_1 is shown (normal mode coordinates given in units of $a_B\sqrt{\text{amu}}$).

between 0 and 0.1 a_B, that is, the coupling to the substrate oscillators will be minimum/maximum at the inner/outer turning point. In Figure 3B, we also show the variance of the wave packet with respect to the reaction coordinate. On average, it amounts to 0.125 a_B, showing that the quantum dynamics takes places in the vicinity of the potential minimum.

As a consequence of the anharmonic couplings in V_{CRS}, the fast oscillations of $\langle x \rangle$ are imposed on the dynamics of $\langle Q_{23} \rangle$ as shown in Figure 3C. The force $f_{23}(x)$ is acting in a way that $\langle Q_{23} \rangle$ is pushed into the negative direction if $\langle x \rangle$ is at the outer turning point. Overall, the excitation of ν_{23} is rather small because of the large frequency mismatch between these two coordinates.

The fast oscillations of $\langle x \rangle$ are low-frequency-modulated most notably with a period of about 500 fs. The latter is a consequence of the anharmonic coupling to the substrate mode ν_1 of which the dynamics is shown in Figure 3D. When panels B and D are compared, it becomes clear that an increase of $\langle Q_1 \rangle$, causing a *compression* of the hydrogen bond, is reflected in a decreased amplitude of $\langle x \rangle$.

A more detailed view of the dynamics is provided by inspection of the populations of zeroth-order states. We have chosen the VD picture of Figure 2 and defined zeroth-order states for the substrate modes according to the shifted oscillator Hamiltonian eq 9, that is, for the nth mode we have the basis set $\{|N_n^{(a)}\rangle\}$. On the basis of these states, one can address the substrate mode interstate and intrastate coupling mediated by the constants $\langle a|K_{mn}(x)|b\rangle$ and $\langle a|K_{mn}(x)|a\rangle$, respectively, as well as the state coupling along a certain normal mode coordinate Q_n having the strength $\langle a|f_n(x)|b\rangle$. It turns out that the coupling linear in Q_n dominates the short-time dynamics.

To illustrate the possible transitions, we neglect the rather small change in frequency for the moment, that is, we set

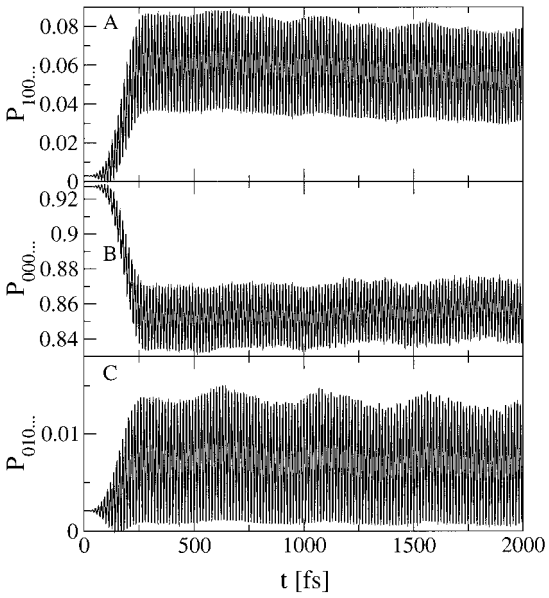

Figure 4. Time evolution of the populations $P_{aN_{23}0...}$ of vibrational ground states in the VD potentials $V_{aa}(\{Q_n\})$ with $a = 1$ (A) and $a = 0$ (B). Panel C shows the respective first excited state along the strongly coupled mode ν_{23}. Pulse parameters are as described in Figure 3.

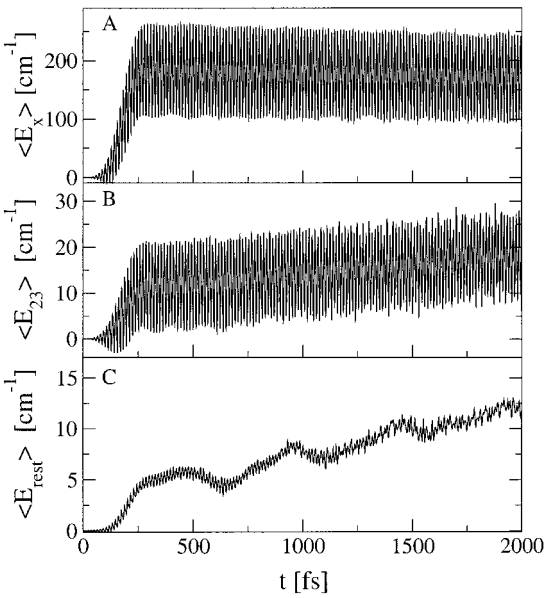

Figure 5. Expectation values for the uncoupled single mode Hamiltonians according to eq 1: (A) reaction coordinate; (B) mode ν_{23}; and (C) remaining seven substrate modes. Pulse parameters are as described in Figure 3.

$\langle a|K_{nn}(x)|a\rangle = \omega_n$. The substrate mode matrix elements for the state coupling $\langle M_n^{(a)}|Q_n|N_n^{(b)}\rangle$ can be calculated straightforwardly using, for instance, the shift-operator method.[30] It follows that

$$\langle M_n^{(a)}|Q_n|N_n^{(b)}\rangle = \sum_{K_n}\sqrt{\frac{\hbar}{2\omega_n}}\mathrm{FC}(M_n,K_n,\Delta g_{ab}) \times \left(\sqrt{N_n+1}\,\delta_{K_n,N_n+1} + \sqrt{N_n}\,\delta_{K_n,N_n-1} - 2g_n(a)\delta_{K_n,N_n}\right) \quad (10)$$

Here, we introduced the dimensionless shift between the VD potential curves as $g_n(a) = -Q_n^{(a)}\sqrt{\omega_n/2\hbar}$ with $Q_n^{(a)}$ being the shifted minimum position in state $|a\rangle$. Further, $\mathrm{FC}(M_n,K_n,\Delta g_{ab})$ is the Franck−Condon overlap integral between two harmonic oscillators displaced by $\Delta g_{ab} = g_n(a) - g_n(b)$ with respect to each other. Because the relative shift of the VD potentials is rather small the Franck−Condon integral will take its maximum value for $M_n = K_n$. This implies that the linear coupling will cause mostly transitions with $\Delta N = \pm 1$.

In Figure 4, we show the populations, $P_{a,N_{23}...}$, for various VD zeroth-order states. Here, the subscript labels the VD state $|a\rangle$ and the respective vibrational quantum number of the most strongly coupled mode ν_{23}. The quantum numbers of the other substrate modes are taken to be zero. In Figure 4A,B, we compare the population dynamics of the vibrational ground states in the two VD states. Here, the state coupling is reflected in the rapid out-of-phase oscillations of $P_{00...}$ and $P_{10...}$. Simultaneously, $P_{01...}$ increases, for example, via an interstate $\Delta N_{23} = -1$ transition as shown in Figure 4C such that its fast oscillations are out-of-phase with the dynamics of $P_{10...}$. The influence of the remaining modes on the OD dynamics leads to low-frequency modulations of the populations shown in Figure 4. In principle, in the VD representation, all substrate modes are vibrationally excited in both VD states. This obscures a clear interpretation of the low-frequency oscillations in, for instance, $P_{10...}$. It should be noted that in terms of the dynamics the population of these vibrationally excited VD states reflects *nuclear wave packet motion* in the different VD potentials of Figure 2B. However, the present situation appears to be more complex than the case of simple vibronic excitation due to the relatively strong interstate coupling.

As an important observation, we notice that the average population $P_{10...}$ in Figure 4A is decreasing with time. At the same time, $P_{00...}$ is increasing. But, both processes take place at a different rate with the decay of $P_{10...}$ being faster. This indicates a complex pattern of vibrational energy redistribution for which the substrate mode−mode coupling terms are also of importance. This view is supported by the behavior of the expectation values $\langle E_{i=x,n}\rangle$ of the uncoupled Hamiltonians eq 1 for the different DOFs. For the reaction coordinate, $\langle E_x\rangle$ in Figure 5A shows an initial increase due to laser excitation and a subsequent slow decay. The fast oscillations are again due to the coupling to the ν_{23} mode as can be seen by comparison with $\langle E_{23}\rangle$ in Figure 5B. The slower modulations apparent in $\langle E_x\rangle$ and $\langle E_{23}\rangle$ are due to the interaction with the remaining seven modes of which the combined total energy $\langle E_{\mathrm{rest}}\rangle$ is shown in Figure 5C. The dynamics of $\langle E_{\mathrm{rest}}\rangle$ is dominated by the mode ν_1 as can be seen from its slow modulation with a period of about 500 fs. Both $\langle E_{23}\rangle$ and $\langle E_{\mathrm{rest}}\rangle$ increase with time as a consequence of intramolecular energy randomization.

It should be stressed that this is clearly a *multiconfiguration effect*, that is, no relaxation-type behavior had been observed in the TDSCF treatment.[16] However, inspecting the natural orbital populations[21] of the different modes, one finds that the leading configurations contribute typically about 90%, thus giving justification for a single configuration treatment of the short-time dynamics.

5. Summary

Combining an ab initio CRS Hamiltonian with MCTDH wave packet propagation, we have investigated the laser-driven dynamics of the medium strength hydrogen bond in PMME-D. The CRS method was demonstrated to have several advantages: (i) A full-dimensional potential surface can be generated, which allows the identification of relevant DOF without prior inspection of all normal modes. While the accuracy of the potential depends on the quality of the Hessian, the mode selection could serve as a starting point for more accurate

calculations in which, for instance, the single-point energies along the normal mode displacements are calculated explicitly.[31] (ii) The CRS Hamiltonian contains all couplings in the potential energy operator. Its factorized form is extremely useful in combination with MCTDH wave packet propagation.

As an application, the intramolecular vibrational dynamics of PMME-D has been treated incorporating the nine most strongly coupled DOF. The anharmonic coupling was shown to trigger vibrational motion of substrate modes after laser pulse excitation of the OD-stretching mode. In view of the recent experiments performed by the Elsaesser group,[14,15] it is most notable that the OD dynamics is modulated by a low-frequency vibration of the hydrogen bond. In refs 14−16, this type of mode was made responsible for the observed oscillations in the IR pump−probe signal. We have analyzed the dynamics in terms of a vibrationally diabatic representation and found a decay behavior of the population in the $\nu_{OD} = 1$ state accompanied by a slow recovery of the $\nu_{OD} = 0$ state population. This is a genuine multiconfiguration effect not seen in the TDSCF calculations. It can be interpreted in terms of intramolecular energy randomization and is also seen in the expectation values for the uncoupled mode Hamiltonians. However, the relaxation time scale for the OD vibration is much longer than the measured T_1 time of 400 fs pointing to the influence of the solvent environment. Preliminary classical dynamics simulations based on the linear response approach[30] support this conclusion.[32] Within the present approach, the effect of the solvent could be modeled using the MCTDH extension to the propagation of density matrices proposed in refs 33 and 34.

Acknowledgment. This work has been supported by the Deutsche Forschungsgemeinschaft through the Sfb450 (H.N. and O.K.). The authors gratefully acknowledge stimulating discussions with J. Dreyer, T. Elsaesser, P. Hamm, D. Madsen, E. Nibbering, and J. Stenger from the Max Born Institute, Berlin.

References and Notes

(1) *Proton transfer in hydrogen-bonded systems*; Bountis, T., Ed.; Plenum Press: New York, 1992.

(2) *Theoretical Treatments of Hydrogen Bonding*; Hadži, D., Ed.; Wiley: Chichester, U.K., 1997.

(3) *Hydrogen Transfer: Experiment and Theory*; Limbach, H.-H., Manz, J., Eds.; Berichte der Bunsen-Gesellschaft 102; Wiley-VCH: Weinheim, Germany, 1998.

(4) Marx, D.; Hutter, J. In *Modern Methods and Algorithms of Quantum Chemistry*; Grotendorst, J., Ed.; NIC Series, Vol. 1; Forschungszentrum Jülich: Jülich, Germany, 2000; p 301.

(5) Carrington, T.; Miller, W.-H. *J. Chem. Phys.* **1984**, *81*, 3941.

(6) Shida, N.; Barbara, P.-F.; Almlöf, J.-E. *J. Chem. Phys.* **1989**, *91*, 4061.

(7) Miller, W.-H.; Handy, N.-C.; Adams, J.-E. *J. Chem. Phys.* **1980**, *72*, 99.

(8) Kraka, E. In *Encyclopedia Computational Chemistry*; von Ragué-Schleyer, P., Ed.; Wiley: New York, 1998; p 2437.

(9) *The reaction path in chemistry: Current approaches and Perspectives*; Heidrich, D., Ed.; Kluwer Academic: Dordrecht, Netherlands, 1995.

(10) Marechal, Y.; Witkowski, A. *J. Chem. Phys.* **1968**, *48*, 3697.

(11) Rösch, N.; Ratner, M. A. *J. Chem. Phys.* **1974**, *61*, 3344.

(12) Robertson, G. N.; Yarwood, J. *Chem. Phys.* **1978**, *32*, 267.

(13) Henri-Rosseau, O.; Blaise, P. *Adv. Chem. Phys.* **1998**, *103*, 1.

(14) Stenger, J.; Madsen, D.; Dreyer, J.; Nibbering, E. T. J.; Hamm, P.; Elsaesser, T. In *Ultrafast Phenomena XII*; Elsaesser, T., Mukamel, S., Murnane, M., Scherer, N., Eds.; Springer Series in Chemical Physics; Springer: New York, 2000; p 542.

(15) Stenger, J.; Madsen, D.; Dreyer, J.; Nibbering, E. T. J.; Hamm, P.; Elsaesser, T. *J. Phys. Chem. A* **2001**, *105*, 2929.

(16) Paramonov, G. K.; Naundorf, H.; Kühn, O. *Eur. J. Phys. D* **2001**, *14*, 205.

(17) McLachlan, A. D. *Mol. Phys.* **1964**, *8*, 39.

(18) Gerber, R. B.; Buch, V.; Ratner, M. A. *J. Chem. Phys.* **1982**, *77*, 3022.

(19) Beck, M. H.; Meyer, H.-D. *Z. Phys. D* **1997**, *42*, 113.

(20) Worth, G. A.; Beck, M. H.; Jäckle, A.; Meyer, H.-D. *MCTDH package*, version 8.2; University of Heidelberg: Heidelberg, Germany, 2000.

(21) Beck, M. H.; Jäckle, A.; Worth, G. A.; Meyer, H.-D. *Phys. Rep.* **2000**, *324*, 1.

(22) Frisch, M. J.; Trucks, G. W.; Schlegel, H. B.; Scuseria, G. E.; Robb, M. A.; Cheeseman, J. R.; Zakrzewski, V. G.; Montgomery, J. A., Jr.; Stratmann, R. E.; Burant, J. C.; Dapprich, S.; Millam, J. M.; Daniels, A. D.; Kudin, K. N.; Strain, M. C.; Farkas, O.; Tomasi, J.; Barone, V.; Cossi, M.; Cammi, R.; Mennucci, B.; Pomelli, C.; Adamo, C.; Clifford, S.; Ochterski, J.; Petersson, G. A.; Ayala, P. Y.; Cui, Q.; Morokuma, K.; Malick, D. K.; Rabuck, A. D.; Raghavachari, K.; Foresman, J. B.; Cioslowski, J.; Ortiz, J. V.; Stefanov, B. B.; Liu, G.; Liashenko, A.; Piskorz, P.; Komaromi, I.; Gomperts, R.; Martin, R. L.; Fox, D. J.; Keith, T.; Al-Laham, M. A.; Peng, C. Y.; Nanayakkara, A.; Gonzalez, C.; Challacombe, M.; Gill, P. M. W.; Johnson, B. G.; Chen, W.; Wong, M. W.; Andres, J. L.; Head-Gordon, M.; Replogle, E. S.; Pople, J. A. *Gaussian 98*, revision A.6; Gaussian, Inc.: Pittsburgh, PA, 1998.

(23) Ruf, B. A.; Miller, W. H. *J. Chem. Soc., Faraday Trans. 2* **1988**, *84*, 1523.

(24) Naundorf, H.; Organero, J. A.; Douhal, A.; Kühn, O. *J. Chem. Phys.* **1999**, *110*, 11286.

(25) Dirac, P. A. M. *Proc. Cambridge Philos. Soc.* **1930**, *26*, 376.

(26) Frenkel, J. *Wave Mechanics*; Clarendon Press: Oxford, U.K., 1934.

(27) Harris, D. O.; Engerholm, G. G.; Gwinn, G. W. *J. Chem. Phys.* **1965**, *43*, 1515.

(28) Light, J. C.; Hamilton, I. P.; Lill, J. V. *J. Chem. Phys.* **1985**, *82*, 1400.

(29) Worth, G. A.; Meyer, H.-D.; Cederbaum, L. S. *J. Chem. Phys.* **1998**, *109*, 3518.

(30) May, V.; Kühn, O. *Charge and Energy Transfer Dynamics in Molecular Systems*; Wiley-VCH: Berlin, 2000.

(31) Orel, A. E.; Zhao, Y.; Kühn, O. *J. Chem. Phys.* **2000**, *112*, 94.

(32) Naundorf, H. Ph.D. Thesis, Freie Universität Berlin, Berlin, Germany, 2001.

(33) Raab, A.; Burghardt, I.; Meyer, H.-D. *J. Chem. Phys.* **1999**, *111*, 8759.

(34) Raab, A.; Meyer, H.-D. *J. Chem. Phys.* **2000**, *112*, 10718.